Molecular Dynamics Study to Identify the Reactive Sites of a Liquid Squalane Surface

Sven P. K. Köhler, Stewart K. Reed,† Robin E. Westacott, and Kenneth G. McKendrick*

School of Engineering and Physical Sciences, Heriot-Watt University, Edinburgh EH14 4AS, United Kingdom

Received: January 20, 2006; In Final Form: April 5, 2006

Molecular dynamics simulations of liquid squalane, $C_{30}H_{62}$, were performed, focusing in particular on the liquid−vacuum interface. These theoretical studies were aimed at identifying potentially reactive sites on the surface, knowledge of which is important for a number of inelastic and reactive scattering experiments. A united atom force field (Martin, M. G.; Siepmann, J. I. *J. Phys. Chem. B* **1999**, *103*, 4508−4517) was used, and the simulations were analyzed with respect to their interfacial properties. A modest but clearly identifiable preference for methyl groups to protrude into the vacuum has been found at lower temperatures. This effect decreases when going to higher temperatures. Additional simulations tracking the flight paths of projectiles directed at a number of randomly chosen surfaces extracted from the molecular dynamics simulations were performed. The geometrical parameters for these calculations were chosen to imitate a typical abstraction reaction, such as the reaction between ground-state oxygen atoms and hydrocarbons. Despite the preference for methyl groups to protrude further into the vacuum, Monte Carlo tracking simulations suggest, on geometric grounds, that primary and secondary hydrogen atoms are roughly equally likely to react with incoming gas-phase atoms. These geometric simulations also indicate that a substantial fraction of the scattered products is likely to undergo at least one secondary collision with hydrocarbon side chains. These results help to interpret the outcome of previous measurements of the internal and external energy distribution of the gas-phase OH products of the interfacial reaction between oxygen atoms and liquid squalane.

Introduction

Liquid−vapor interfaces play an important role in many processes in chemical, biological, material, and environmental science. A detailed knowledge of the structure of the surface at a molecular level is important to understand processes such as distillation, particle exchange at the surface of the sea, mass accumulation on atmospheric aerosols,[1,2] and generally reactions at interfaces.[3] Some experimental techniques are available to obtain information about the structure and orientation of molecular groups. However, they have mainly been applied to investigate processes that exhibit a certain degree of order at the surface. These include, to name a few, the phenomenon of surface freezing[4,5] or the ordering of surfactants on surfaces.[6,7] We report here a theoretical investigation into the molecular structure of the surface of pure liquid squalane, $C_{30}H_{62}$, where the principal interest is to derive information about potentially reactive sites on the liquid surface.

Squalane (2,6,10,15,19,23-hexamethyltetracosane) is a liquid hydrocarbon consisting of a C_{24} backbone with six symmetrically placed methyl groups. It has a very low vapor pressure (less than 1×10^{-7} Torr), which makes it an ideal candidate for reaction dynamics experiments performed under (ultra) high vacuum. This was first exploited by Nathanson and co-workers and subsequently by other groups, so that squalane has become something of a benchmark molecule for gas−liquid dynamics studies. Nathanson and co-workers performed inelastic scattering experiments of rare gas atoms from liquid squalane surfaces.[8] It was found that the scattered atoms leave the surface with a bimodal kinetic energy distribution. The direct component, which scatters at near specular angles, has a kinetic energy close to the impinging atoms. The thermal component, whose angular distribution is randomly distributed around the surface normal, has a kinetic energy distribution that can be described by a Boltzmann distribution at or near the temperature of the surface.

This work was followed by molecular-beam based reactive scattering experiments between ground-state oxygen atoms, $O(^3P)$, and a liquid squalane surface by Minton and co-workers, initially in cooperation with Casavecchia's group.[9] They found that reactively scattered gas-phase products also show a bimodal translational energy distribution with direct and thermal (or trapping−desorption) components. Complementary spectroscopic experiments by McKendrick and co-workers focused on the internal energy distribution of the reactive OH radical, deriving rotational distributions and vibrational branching ratios as a function of liquid surface temperature and flight time of the OH radicals.[10] For the interpretation of all the previous experiments, it is key to know with which atoms or segments of the squalane molecules the incoming atoms collide. This is because different reactive sites on liquid squalane can yield different internal energy distributions. For example, it is known from experiments in the homogeneous gas phase that the vibrational branching ratio $(v' = 1)/(v' = 0)$ varies for the reaction between $O(^3P)$ atoms and primary, secondary, and tertiary hydrogen atoms on saturated hydrocarbons in the order $\leq 1\%$, $\sim 25\%$, to $\sim 150\%$.[11,12] A vibrational branching ratio of $\sim 10\%$ found in the reaction between $O(^3P)$ and liquid squalane is therefore suggestive that the oxygen atoms do react with various different hydrogen atoms.[10] In addition, the external energy distribution of the scattered species may also be

* Corresponding author. E-mail: k.g.mckendrick@hw.ac.uk.
† Present address: School of Chemistry, University of Edinburgh, West Mains Rd., Edinburgh EH9 3JJ, UK.

10.1021/jp060431p CCC: $33.50
Published on Web 06/01/2006

influenced by the structure of the immediate environment of the reaction site. A very rough surface increases the possibility that the scattered products hit one or more side chains after reaction on the surface. This may result in a kinetic energy distribution closer to what would be expected from a Boltzmann distribution at the surface temperature. There would be a corresponding effect on the rotational energy distributions. Conversely, an atomically flat surface increases the ratio of products that scatter back directly into the gas phase. It is therefore desirable to understand the structure of a liquid surface at a molecular level.

Molecular dynamics (MD) simulations by Harris[13] have regularly been cited as an indicator of the structure of a liquid hydrocarbon surface. It is important, however, to note that Harris investigated the liquid hydrocarbons *n*-decane and *n*-eicosane, $C_{10}H_{22}$ and $C_{20}H_{42}$, both of which are linear in structure. A slight preference of the methyl groups to protrude into the vacuum was found. In the absence of any other information, this has been interpreted as an indication that the attacking oxygen atoms might preferentially react with the primary hydrogen atoms of squalane.[9] There have been a number of simulation studies that focused on squalane itself but did not explicitly investigate the gas−liquid interface. They concentrated on reproducing bulk properties such as diffusion coefficients and end-to-end distances and phase-changing properties such as the liquid−vapor coexistence curve.[14,15] The sole exception is a study by Siepmann and co-workers, who did investigate the liquid−vapor interface. They investigated a slab of 96 squalane molecules with two liquid−vapor interfaces. They used a Monte Carlo method[16] as distinct from the MD simulations we perform here. The derived *z*-density profiles, which depict the rise in density of the different hydrocarbon segments (CH, CH_2, and CH_3) when going from the vacuum to the bulk, were not interpreted explicitly as showing a preference for any of the groups to protrude into the vacuum.

The results of our own previous experiments regarding the vibrational branching ratio[10] can be interpreted to indicate that oxygen atoms do not react exclusively with primary hydrogen atoms, but also with secondary and/or tertiary H atoms, at the squalane surface. This formed the motivation for us to investigate further the structure of the liquid squalane interface at a molecular level and attempt to identify the reactive sites at the surface. The Materials and Methods describes the methodology used in the molecular dynamics simulations presented here. The Results and Discussion reports and discusses the results, in particular the *z*-densities for the different hydrocarbon segments, and shows a snapshot of the surface. We also derived information about the likelihood of incoming atoms hitting different segments of the squalane molecules on the surface. The angular distribution of the incoming atoms in these calculations was chosen to model the distribution of oxygen atoms in our own previous experiments. Flight paths were sampled from such a distribution of oxygen atoms and tracked on their way to the surface. The main results are summarized in the Conclusion.

Methods

The TraPPE (transferable potential for phase equilibria) force field developed by Siepmann and co-workers specifically for branched alkanes was used in these simulations.[17] All CH_3, CH_2, and CH units were treated as pseudo-atoms (united atom model) (i.e., hydrogen atoms are not explicitly considered). We chose this particular force field over others available[14,18] as it reproduces the phase behavior of hydrocarbons very well.[17]

TABLE 1: Parameters of the TraPPE Force Field Taken from Ref 17

bond length		r_0/Å	
CH_x-CH_y		1.54	
bend	θ_0/deg	k_θ/kJ mol^{-1}	
$CH_x-CH_2-CH_y$	114	519.66	
$CH_x-CH(CH_3)-CH_y$	112	519.66	
torsion	c_1/kJ mol^{-1}	c_2/kJ mol^{-1}	c_3/kJ mol^{-1}
$CH_x-CH_2-CH_2-CH_y$	2.7856	−0.5670	6.5794
$CH_x-CH_2-CH(CH_3)-CH_y$[a]	3.5647	−0.9300	3.6689
pseudo-atom	ϵ_{ij}/kJ mol^{-1}		σ_{ij}/Å
CH_3	0.8148		3.75
CH_2	0.3825		3.95
CH	0.0831		4.68

[a] The original form of this torsional potential contains an additional constant $c_0 = -2.087$ kJ mol^{-1}, which has been omitted here.

The force field constrains all C−C bonds to 1.54 Å. Bond angle bending is described by a harmonic potential of the form

$$U(\theta) = \frac{1}{2}k_\theta(\theta - \theta_0)^2 \tag{1}$$

where k_θ is the force constant and θ_0 is the equilibrium angle. Their values are given in Table 1. The torsional potential is described by

$$U(\phi) = c_1[1 + \cos\phi] + c_2[1 - \cos(2\phi)] + c_3[1 + \cos(3\phi)] \tag{2}$$

where ϕ is the dihedral angle and constants c_1, c_2, and c_3 are given in Table 1. The original force field by Siepmann includes a ϕ-independent constant, c_0, with a value of -2.087 kJ mol^{-1}, in the torsional term for only the $CH_x-(CH_2)-CH(CH_3)-CH_y$ dihedral angle. We omit this constant here. This has no effect on the gradients of the potential and hence the resulting forces that are used in a MD simulation. The nonbonding interaction between pseudo-atoms of different molecules or between atoms in the same molecule separated by more than three bonds (i.e., whose interaction is not governed by bond constraints, angular potentials, or dihedral potentials) is described by the Lennard−Jones 12-6 potential

$$U(r_{ij}) = 4\epsilon_{ij}\left[\left(\frac{\sigma_{ij}}{r_{ij}}\right)^{12} - \left(\frac{\sigma_{ij}}{r_{ij}}\right)^{6}\right] \tag{3}$$

As is standard, r_{ij} is the distance, σ_{ij} is the Lennard−Jones contact distance, and ϵ_{ij} is the well depth, given in Table 1. For interactions between unlike pseudo-atoms, Lorentz−Berthelot combining rules are applied

$$\sigma_{ij} = \frac{1}{2}(\sigma_{ii} + \sigma_{jj}) \tag{4}$$

$$\epsilon_{ij} = \sqrt{\epsilon_{ii}\epsilon_{jj}} \tag{5}$$

Interatomic forces are truncated after 12 Å.

All simulations were performed in the *NVT* ensemble using the molecular dynamics program DL_POLY.[19] The SHAKE algorithm was used to constrain the carbon−carbon bonds to be 1.54 Å. The temperature was regulated by a Nosé−Hoover thermostat with a relaxation constant of 1 ps.[20] Simulations were started from two very different starting configurations as

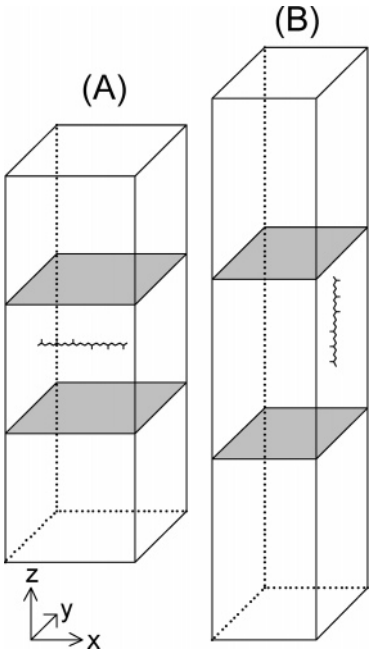

Figure 1. Illustration of the two different starting configurations. Initial interfaces are gray. Configuration A contains 288 ($2 \times 12 \times 12$) molecules all arranged parallel to the interface in a box $64.68 \times 64.8 \times 185.58$ Å^3. Configuration B contains 324 ($9 \times 9 \times 4$) molecules perpendicular to the interface in a box $48.6 \times 46.395 \times 388.08$ Å^3. The overall length of the *z*-dimension is three times the length between the interfaces (i.e., two-thirds of the box is not filled with molecules). The single molecules shown schematically are only intended to illustrate the initial orientation of all molecules in the box and are not drawn to scale.

illustrated in Figure 1. The first configuration, which will be referred to as configuration A from now on, consisted of 288 squalane molecules, all of which were initially arranged parallel to the interface. Simulations with 324 molecules perpendicular to the interface (configuration B) were also performed to test whether the initial structure has an influence on the results. The dimensions of the box were chosen so that the number of molecules between the interfaces matches the bulk density of squalane of 0.81 g cm^{-3}. The molecules initially take up one-third of the volume of the whole box. Periodic boundary conditions were applied in all directions.

Results and Discussion

The MD simulations using configuration A were run for 1.5 ns at 298 K, then for 0.6 ns at 400 K, and again at 298 K for a further 1.0 ns. The simulations using configuration B were initially run for 2.1 ns at 298 K, then heated to 500 K for 1.0 ns, and returned to 298 K for 1.3 ns. None of the simulations showed any signs of molecules evaporating into the vacuum. The configurational energy, E_{config}, was found to converge toward the same value for configurations A and B, suggesting that both simulations reach equilibrium. For the purposes of establishing the statistical properties of the surface, only those periods after E_{config} had stabilized have been analyzed further. They were chosen to exclude the first 100 ps after each temperature change.

Another probe of the equilibration of the system is to calculate the distribution of the polar and azimuthal angles, θ and φ, between each C−C bond and the space-fixed coordinate system. Because of the highly ordered starting configuration, only a narrow range of angles is populated initially. The distribution of angles during the periods selected for analysis was found to

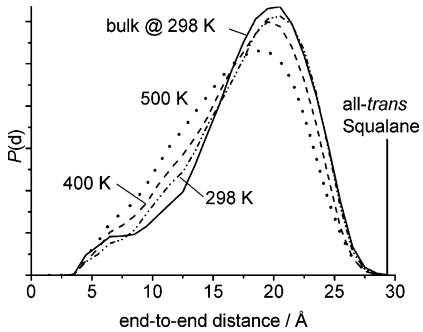

Figure 2. Normalized end-to-end distributions for simulations containing two interfaces at 298 K (dash−dotted line), 400 K (dashed line), and 500 K (dotted line) in comparison with a bulk simulation at 298 K (solid line). The vertical solid line indicates the length of an all-trans squalane molecule, as in the starting configuration.

be effectively completely random (i.e., as required for equilibration, the squalane molecules have no memory of their starting configuration).

To further validate the appropriateness of the force field and demonstrate equilibration of the simulation, we have also calculated the surface tension. This can be compared with experimental values. The approximate formula for the surface tension previously used by Kvamme and co-workers[21] was applied

$$\gamma = 0.5 h_z \left\{ \bar{P}_z - \frac{1}{2}[\bar{P}_x + \bar{P}_y] \right\} \tag{6}$$

where h_z is the length of the simulation box in the *z*-direction. P_x, P_y, and P_z are the *x*-, *y*-, and *z*-components of the pressure tensor. The factor of 0.5 accounts for the fact that there are two interfaces present. The pressure tensor has been captured at intervals of 1 ps between 2.2 and 3.1 ns for configuration A and at intervals of 100 fs between 3.3 and 4.4 ns for configuration B. Taking statistical inefficiency into account, surface tensions, γ, of (25.9 ± 2.9) mN m^{-1} and (25.6 ± 2.7) mN m^{-1} were obtained for configurations A and B, respectively. These are in good agreement with experimental values, which vary in the literature between 28 and 30 mN m^{-1}.[8a,22]

We also calculated the distribution of the distance between the first and the last united atom (end-to-end distance) of each molecule. As can be seen in Figure 2, virtually no molecules remain in a fully stretched configuration. There seems to be a preference for the molecules to be in a more folded configuration at higher temperatures as might intuitively be expected. For the purposes of this comparison, we carried out separate MD simulations of bulk squalane at 298 K. The end-to-end distance in the bulk is shifted slightly away from smaller values as compared to the simulations at the same temperature that include the two interfaces. This indicates that the molecules at the interface are more inclined to fold over on themselves than in the bulk, which is also in line with expectations. We find a mean end-to-end distance in the bulk at 298 K of ∼18 Å, in good agreement with previous work by Grest and co-workers.[14]

z-Density profiles are density distributions of the center points of united atoms. They can deliver information about the structure of the liquid surface, the principal aim of this study. A preference for a particular segment of the squalane molecule to protrude into the vacuum can be identified if the *z*-density profiles are plotted for each segment (CH_3, CH_2, and CH) separately. To aid the comparison of profiles, the total density change of all carbon atoms at the gas−liquid interfaces was fitted to the standard formula,[23,24] allowing the simulations at different

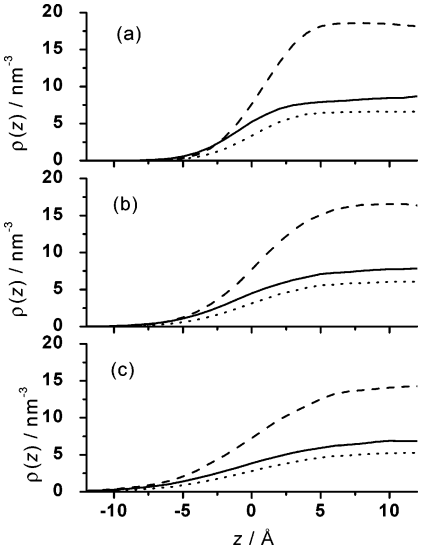

Figure 3. *z*-Density plots for equilibrated simulations (a) at 298 K (with initial configuration A), (b) at 400 K (initial configuration A), and (c) the equilibrated simulations at 500 K with configuration B. Solid lines are primary, dashed lines secondary, and dotted lines tertiary united carbon atoms.

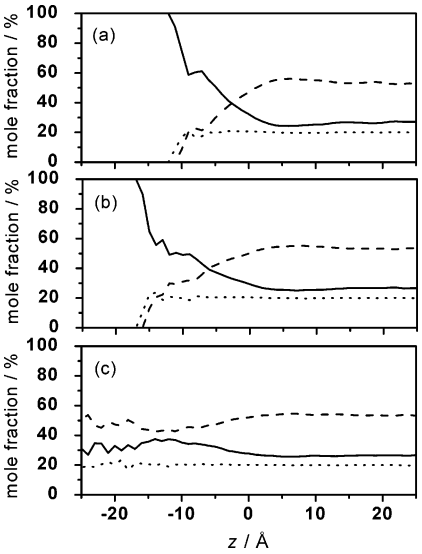

Figure 4. Mole fraction of the respective carbon atoms across the interface for (a) simulations at 298 K using configuration A, (b) at 400 K using configuration A, and (c) at 500 K using configuration B. Solid lines are primary, dashed lines secondary, and dotted lines tertiary carbon atoms.

temperatures to be shifted so that the Gibbs dividing surface was located at a common zero. Figure 3 depicts the shifted but otherwise raw *z*-density plots of the three different united atoms of squalane at temperatures of 298, 400, and 500 K.

Most interestingly, one can see from Figure 3 that the methyl groups have a modest but clearly discernible preference to protrude from the surface at lower temperatures. This shows up as an earlier onset of the methyl group density as compared with the CH_2 and CH groups in panels a and b. In fact, the density of the CH_3 groups exceeds those of the CH_2 groups up to a point ~2.5 Å outside the Gibbs dividing surface for simulations at 298 K. The different densities in the bulk simply reflect the ratio of secondary to primary to tertiary carbon atoms of 16:8:6. The preference for the methyl groups to protrude into the vacuum can be seen more clearly in Figure 4, which depicts the mole fraction of a particular type of carbon atom on moving

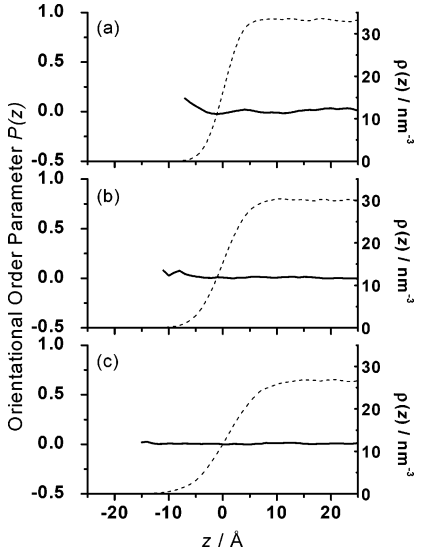

Figure 5. Orientational order parameter $P(z)$ for the first five 1−3 carbon−carbon vectors of each end of the squalane molecules (solid line) in relation to the overall *z*-density profiles (dashed line) for equilibrated simulations at (a) 298 K (initial configuration A), (b) 400 K (initial configuration A), and (c) 500 K (initial configuration B).

from the vacuum into the bulk. This preference is more pronounced at 298 K than at 400 K and effectively lost at 500 K.

A qualitatively similar preference was also detected by Harris in his work on $C_{10}H_{22}$ and $C_{20}H_{42}$, as was the diminishing effect with increasing temperature.[13] Wick et al. did not identify an excess of methyl groups protruding into the vacuum.[16] However, if their *z*-density plot (Figure 2 of ref 16) is scaled by the number of CH_3, CH_2, and CH groups, it is possible to make out a very subtle preference for the methyl groups.

Continuing the analysis of the structure of the interface, we show in Figure 5 the overall *z*-density profiles at different temperatures. These are the sum of densities of the three different united atoms. It can be seen that the interface, which is ~6 Å wide at 298 K, becomes wider with increasing temperature. This enlargement has also been observed in previous MD simulations of liquid hydrocarbons and is as intuitively expected for an increase on local disorder and looser packing at higher temperatures.

Also superimposed in Figure 5 is the orientational order parameter $P(z)$, which is defined as

$$P(z) = {}^1/_2[3(\cos^2\theta) - 1] \tag{7}$$

where θ is the angle between the *z*-axis (perpendicular to the interface) and a vector connecting two carbon atoms, which are two units apart (e.g., atoms 1 and 3). Being mainly interested in the orientation of the chain ends, we calculated θ for the first five such carbon−carbon vectors starting from each end of the molecule and assigned a *z*-value that corresponds to the midpoint between the two atoms; see Figure 6. The orientational order parameter was then calculated, and the average was taken for all parameters that fell within a given interval (usually taken in 1 Å steps) along the *z*-axis.

$P(z)$ is expected to be +1 if all vectors are aligned perpendicular to the interface and −0.5 if all vectors are parallel to the interface. It can be seen from Figure 5 that there is no significant order within the bulk, with $P(z)$ effectively zero, as would intuitively be expected. Moving outward past the Gibbs dividing surface, there is an apparent slight preference for some

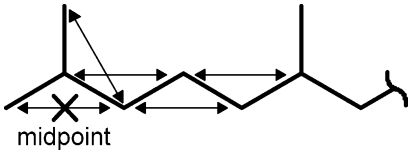

Figure 6. Illustration of the five 1−3 vectors used to calculate the orientational order parameter. The same vectors have also been used at the other end of each molecule. One representative midpoint is indicated.

chain ends to adopt an upright orientation. However, this is not especially surprising because when the densities drop to such low values, single chains can only reach this far out from the surface when they happen to be aligned more or less perpendicular to the interface. The extent of this slight effect does again appear to decline with temperature, consistent with an increase in local disorder.

It is clear from the previous analysis that there is a modest preference for methyl groups to protrude further from the surface than the secondary and tertiary groups. This is more pronounced at lower temperatures. It is not so straightforward to deduce, though, on the basis of the average *z*-density profiles alone, the extent to which this would mean that an incoming projectile would be biased toward collisions with a CH_3 group. A qualitative alternative is to view the surface from the perspective of an incoming projectile. This is illustrated in the snapshot of the surface viewed along different axes in Figure 7. Hydrogen atoms are now included by retrospectively placing them in a tetrahedral environment of the respective carbon atom, avoiding staggered interactions.

This single configuration has the same characteristics with regards to its *z*-density as the average of configurations shown in Figure 3. The surface appears by no means atomically flat. Significantly, it can be seen that although the primary carbon and hydrogen atoms take up a significant part of the visible outer surface area, they by no means cover all of it.

In an attempt to determine more quantitatively which site an incoming atom or molecule will collide with, we carried out simple Monte Carlo tracking of straight-line trajectories directed at surfaces. The surfaces were selected randomly from the equilibrated intervals of the MD simulations. We assumed that an incoming atom (which in the case of our own experiments would be oxygen) is created in a 20 × 20 × 20 Å^3 cube that has its center located 50 Å above the central section of the target surface. This surface has dimensions 64.68 × 64.8 Å^2 for configuration A and 48.6 × 46.395 Å^2 for configuration B. The angle θ between the flight path and the *z*-axis of the coordinate system was Monte Carlo selected from a distribution of angles given by the term

$$P(\theta) = \frac{1 + \beta P_2(\cos\theta)}{4\pi} \qquad (8)$$

where P_2 is the second-order Legendre polynomial in cos θ. The β parameter for the 355 nm photolysis of NO_2 at room temperature is 0.7.[25] The projectile is assumed to collide with the first atom of any kind for which the closest distance of approach is less than a selected value. These were taken in separate simulations to be 2.0, 2.5, or 3.0 Å, respectively. It is known from simulations of the gas-phase reaction between O(^{3}P) and CH_4 that the O−H distance at the transition state is ∼1.2 Å.[26] The incoming oxygen atom and the hydrogen atom start to interact, however, at much greater distances. We therefore believe that the contact distances selected are a reasonable choice to cover the range of distances at which inelastic or reactive scattering might occur. In any event, the probability for colliding with a primary, secondary, or tertiary hydrogen atom was found in practice not to show a significant correlation with the choice of this distance. We present therefore the average results over the three selected distances. For each temperature, flight path sampling was performed on three different configurations chosen randomly from all simulation times during the equilibrium period, and the results were averaged. The resulting average collision probabilities for different temperatures are listed in Table 2. (The total probability is obviously normalized because all incoming atoms inevitably collide with some part of the liquid.)

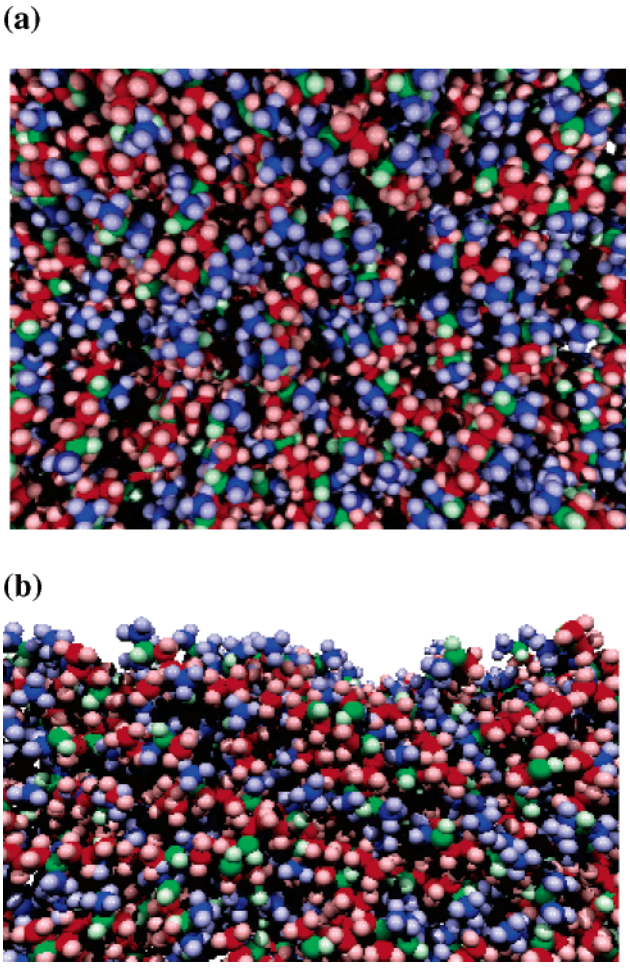

Figure 7. Snapshot of the liquid squalane surface at 298 K after 3.1 ns (configuration A). Dark blue spheres are primary carbon atoms, red spheres are secondary, and green spheres are tertiary carbon atoms. Hydrogen atoms, inserted retrospectively, are represented in the respective lighter color. (a) Plan view along *z*-axis and (b) side view along *y*-axis.

TABLE 2: Probability of an Incoming Projectile Colliding with a Primary, Secondary, or Tertiary Hydrogen Atom on Squalane, Averaged Over the Three Contact Distances 2.0, 2.5, and 3.0 Å

T_{surf}/K	primary H	secondary H	tertiary H
298	0.41	0.50	0.09
400	0.42	0.48	0.10
500	0.45	0.48	0.07

It can be seen from Table 2 that the probability of colliding with different hydrogen atoms is qualitatively not much different from the abundance of primary, secondary, and tertiary hydrogen atoms in squalane (0.39:0.51:0.10). In other words, the slight enrichment of the methyl groups in the outer parts of the surface,

TABLE 3: Overall Probability for Colliding in a Potentially Reactive Geometry for Different Acceptance Angles, Averaged over Primary, Secondary, and Tertiary Hydrogen Atoms[a]

T_{surf}/K	$\alpha_{accp} = 30°$	$\alpha_{accp} = 37.5°$	$\alpha_{accp} = 45°$
298	8%	16%	19%
400	13%	22%	30%
500	18%	18%	21%

[a] α_{accp} is the allowed deviation from the preferred angle of 180°.

TABLE 4: Ratios of Reactive Collisions Occurring with Primary, Secondary, or Tertiary Hydrogen Atom Averaged Over All Acceptance Angles

T_{surf}/K	primary H	secondary H	tertiary H
298	0.45	0.46	0.09
400	0.41	0.50	0.09
500	0.57	0.37	0.06

identified previously, has relatively little influence over the type of group first encountered. There is also no obvious strong variation with temperature.

Since we are particularly interested in hydrogen abstraction by an oxygen atom, we attempted to establish the likelihood that the collision reaches a potentially reactive configuration, in geometric terms, and hence has the capacity to lead to the production of OH. We neglect from the current discussion any consideration of the variation of the energetic barrier heights with the nature of the C−H bond. It is simply not possible to do this in any straightforward way in this simple model that therefore examines solely the geometric accessibility of different atoms. It is well-known from the corresponding gas-phase reaction that the abstraction mechanism takes place preferentially when the C−H−O angle is around 180° since the reaction barrier increases significantly with decreasing angle.[26] The geometric properties of the transition state are not expected to vary substantially for primary, secondary, and tertiary C−H sites. We therefore assumed in our model that the collision of an oxygen atom with a hydrogen atom is only reactive if the C−H−O angle did not deviate from 180° by more than a selected angle. Once again, a range of values for this cone-of-acceptance angle (30.0, 37.5, and 45.0°) was selected to establish its influence. In practice, we found no statistically significant effect of the specific value of the acceptance angle on the ratio between potentially reactive collisions with primary, secondary, and tertiary hydrogen atoms. We therefore present in Table 3 the probability of reaching a potentially reactive geometry for different cone-of-acceptance angles, averaged over the three different hydrogen atom types. Not surprisingly, the absolute probability for a collision to be potentially reactive (which is no longer normalized to unity) is found to depend on the acceptance angle, with the predictable increase in the reaction probability as the angular constraint is relaxed. With the increased statistical scatter resulting from the reduced number of trajectories satisfying the angular condition (3150 in total over the three temperatures), it would probably not be meaningful to infer any firm conclusions about the temperature dependence of the reaction probability.

Perhaps more interesting is the relative number of reactive trajectories, averaged over the acceptance angles but separated into primary, secondary, and tertiary contributions. The results, given in Table 4, appear to show that the requirement to reach a specific geometry has had a slight influence over the relative likelihood of reaction, as opposed to the total rate of collisions (Table 2), with the different atom types. The primary atoms have gained relatively, such that it is now roughly equally probable that a potentially reactive configuration will be reached with a secondary or a primary hydrogen atom. We interpret this to indicate that primary hydrogen atoms are, on average, directed more favorably toward the incoming atom than secondary hydrogen atoms.

It seems clear from the previous analysis that an incoming oxygen atom is very likely to be able to collide (and potentially react) with all three of the different hydrogen atom types. A note of caution is therefore appropriate in general not to overinterpret differences between atom types in the *z*-density plots. A connection can be made between the predictions and the results of real experiments, although the obvious limitations of the current model should be borne in mind, particularly the omission of any dependence of barrier height on atom type. As noted previously, it is known from previous experiments between $O(^3P)$ and gas-phase hydrocarbons that the reaction with primary hydrogen atoms effectively does not yield vibrationally excited OH radicals, whereas reaction with secondary and tertiary hydrogen atoms yields significant amounts of $OH(v' = 1)$. The predicted accessibility of secondary and tertiary hydrogen atoms on the liquid surface to incoming oxygen atoms is therefore consistent with the experimental observation of a moderate fraction (around 10%) of vibrationally excited OH radicals in the reaction between $O(^3P)$ and a liquid squalane surface.

Turning to the fate of the departing OH radical, we attempted to quantify the ratio of hydroxyl radicals that, on their flight path away from the surface, could potentially undergo secondary collisions with side chains of surface squalane molecules. The purpose was to allow some qualitative comparison with the ratio between the direct and the thermal components of OH translational and rotational distributions inferred from previous gas−liquid interfacial experiments. As a first step, the aim was to evaluate, on a purely geometric basis, how surrounded the nascent OH is at the point it is formed in the interfacial zone. To proceed, it is necessary to make some further assumptions about the angular scattering of the product OH. In this first elementary model, we did not include any memory of the incoming trajectory and assume that the OH is predominantly backscattered. This is based on the well-established constraint to near collinearity in the gas phase, discussed previously. This will favor backscattering, at least for collision energies that do not substantially exceed the barrier height. The distribution was modeled by a $\cos^4 \theta$ dependence around the C−H bond from which the H atom is abstracted. The OH radical was treated as a sphere. If it passed within a certain critical distance of any atom on its return journey, other than the carbon atom from which the H atom was abstracted, it was counted as having undergone a collision. Flight paths were not tracked any further from this point. The result is the ratio of OH radicals that would have undergone at least one collision, with the implication that they may suffer further collisions and ultimately may thermalize. These estimates are likely to represent lower limits on the true probability because a broader angular scattering distribution is obviously likely to increase the chance of a secondary collision.

The critical value of the distance was taken representatively in separate runs to be less than 2.0, 2.5, or 3.0 Å, respectively. We sampled 50 outgoing flight paths for each of the 3150 incoming successful trajectories identified previously. The results are shown in Table 5.

The probability of undergoing a secondary collision is found to depend on all three parameters: the critical distance for reaction of an incoming oxygen atom, the acceptance angle for reaction, and the critical distance for collisions between the OH

TABLE 5: Range of Probabilities that Departing OH Radical Undergoes at Least One Collision with a Segment of Surface Squalane Molecules[a]

T_{surf}/K	O(^{3}P) critical distance for reaction 2.0, 2.5, 3.0 Å	acceptance angle 30.0°, 37.5°, 45.0°	OH critical distance for secondary collision 2.0, 2.5, 3.0 Å
298	87, 80, 76%	81, 87, 85%	62, 87, 89%
400	80, 69, 74%	75, 80, 84%	49, 80, 85%
500	81, 83, 72%	82, 81, 83%	71, 81, 88%

[a] Each parameter was varied independently with the other two held fixed.

radical and the hydrocarbon chains. A larger oxygen distance for an oxygen atom reaction causes a lower OH secondary collision ratio. This is not surprising since there is clearly a reduced chance of a secondary collision of the recoiling OH if the potentially reactive collision takes place further away from the bulk. More subtly, a larger acceptance angle for reaction with oxygen atoms appears to cause a slight increase in the chance of secondary OH collisions, at least for the two lower temperatures. If a real effect, this is presumably because it allows reactive collisions with less accessible C−H bonds, which on average are less inclined along the surface normal and may lie deeper in the surface. Both factors would enhance the chance of a secondary collision of the recoiling OH. A larger OH critical distance increases the fraction of secondary collisions for obvious reasons. We do not detect, in any case, a strong correlation with surface temperature.

Relating this to our own previous experiments, we have recorded rotational state distributions and time-of-flight profiles of the OH radicals.[10b] Measurements of the OH rotational temperature at different liquid surface temperatures and delay times were taken to indicate clearly that some hydroxyl radicals thermalize at the liquid surface. Forward Monte Carlo simulations reproduced the experimental time-of-flight profiles very well. Best agreement was reached when a contribution from the thermal component of 60% was assumed. We do not expect an accurate quantitative agreement between the experiment and the current simple model. Nevertheless, it is encouraging that the prediction, for a range of plausible sets of model parameters, that the majority (in most cases lying in the range of 70−80%) of OH radicals make at least one secondary collision is at least qualitatively consistent with the experimental observation that a significant fraction get trapped at the surface. Of course, the exact fraction of the thermal component will depend strongly on the incident energy and angle, as Minton and co-workers have shown.[9] They found the direct component to become more pronounced as the incident energy gets higher and the incident angle becomes lower.

Conclusion

Relatively large-scale molecular dynamics simulations of liquid squalane, $C_{30}H_{62}$, were performed using an established force field. After equilibration of the system, various interfacial parameters were derived. The surface tension was found to be $\gamma = (25.6 \pm 2.7)$ mN m^{-1} in fairly good agreement with experimental values. As for the structure of the interface, a modest preference for the methyl groups to protrude from the surface has been found at lower temperatures. This effect diminishes at higher temperatures. We note that this is a valuable result that could be of interest in a number of fields extending beyond the current specific focus on interfacial reaction dynamics. The width of the interface increases with increasing temperature. No significant degree of surface ordering could be detected beyond what is expected for a gradual decrease of density at the interface.

A purely geometric tracking model was developed to attempt to quantify the ratio of primary, secondary, and tertiary atom types with which an incoming atom or molecule could scatter or react. The slight preference of the primary atoms to protrude from the surface does not in itself significantly enhance the chance of their being impacted by incoming atoms. However, when an angular constraint is imposed on reactivity, it may result in a modest bias toward the primary atoms. Nevertheless, all three atom types are predicted to be significantly accessible to incoming projectiles. This is consistent with the experimental observation of an OH vibrational branching ratio of around 10% in the reaction between O(^{3}P) and a liquid squalane surface appearing to require at least a component of the reaction to take place with secondary or tertiary hydrogen atoms. The model was extended to predict the fraction of OH molecules that might undergo a secondary collision before escaping the surface. On the basis of reasonable assumptions, it is predicted that the majority would do so. This is also consistent with experimental observations that a significant proportion of the OH adopts thermal translational and rotational distributions close to the surface temperature.

The simple model described previously has been constructed on a purely geometric basis and neglects completely energetic effects in the entrance channel, along with considerations of momentum conservation for the directly scattered products. It would, however, be interesting to model the reaction between oxygen atoms and liquid squalane surface more rigorously. Given the size of the system, it might be feasible to carry out scattering calculations in a QM/MM fashion (i.e., treating the reaction center quantum mechanically and the remaining bulk in a molecular mechanics fashion). This has been done successfully for the related reaction between O(^{3}P) and self-assembled monolayers of alkyl chains[27] and would clearly be an interesting extension of the current work.

Acknowledgment. The authors thank EPSRC for a research grant and the EPSRC National Service for Computational Chemistry Software for provision of computer time on the Columbus cluster at the Rutherford-Appleton Laboratory. S.P.K.K. thanks the Verband der Chemischen Industrie for a scholarship. Mhairi Allan performed the experimental measurements of the vibrational branching ratio with which model comparisons were made.

References and Notes

(1) Ellison, G. B.; Tuck, A. F.; Vaida, V. *J. Geophys. Res.* **1999**, *104*, 11633−11641.

(2) Molina, M. J.; Molina, L. T.; Kolb, C. E. *Annu. Rev. Phys. Chem.* **1996**, *47*, 327−367.

(3) Nathanson, G. M. *Annu. Rev. Phys. Chem.* **2004**, *55*, 231−255.

(4) Wu, X. Z.; Sirota, E. B.; Sinha, S. K.; Ocko, B. M.; Deutsch, M. *Phys. Rev. Lett.* **1993**, *70*, 958−961.

(5) Sefler, G. A.; Du, Q.; Miranda, P. B.; Shen, Y. R. *Chem. Phys. Lett.* **1995**, *235*, 347−354.

(6) Watry, M. R.; Tarbuck, T. L.; Richmond, G. L. *J. Phys. Chem. B* **2003**, *107*, 512−518.

(7) Miranda, P. B.; Shen, Y. R. *J. Phys. Chem. B* **1999**, *103*, 3292−3307.

(8) (a) Saecker, M. E.; Govoni, S. T.; Kowalski, D. V.; King, M. E.; Nathanson, G. M. *Science* **1991**, *252*, 1421−1424. (b) Saecker, M. E.; Nathanson, G. M. *J. Chem. Phys.* **1993**, *99*, 7056−7075.

(9) (a) Garton, D. J.; Minton, T. K.; Alagia, M.; Balucani, N.; Casavecchia, P.; Volpi, G. G. *Faraday Discuss. Chem. Soc.* **1997**, *108*, 387−399. (b) Garton, D. J.; Minton, T. K.; Alagia, M.; Balucani, N.; Casavecchia, P.; Volpi, G. G. *J. Chem. Phys.* **2000**, *112*, 5975−5984. (c) Garton, D. J.; Minton, T. K.; Alagia, M.; Balucani, N.; Casavecchia, P.; Volpi, G. G. *J. Chem. Phys.* **2001**, *114*, 5958.

(10) (a) Kelso, H.; Köhler, S. P. K.; Henderson, D. A.; McKendrick, K. G. *J. Chem. Phys.* **2003**, *119*, 9985−9988. (b) Köhler, S. P. K.; Allan, M.; Kelso, H.; Henderson, D. A.; McKendrick, K. G. *J. Chem. Phys.* **2005**, *122*, 24712. (c) Köhler, S. P. K.; Allan, M.; Costen, M. L.; McKendrick, K. G. *J. Phys. Chem. B* **2006**, *110*, 2771.

(11) Andresen, P.; Luntz, A. C. *J. Chem. Phys.* **1980**, *71*, 5842−5850.

(12) Ausfelder, F.; McKendrick, K. G. *Prog. React. Kinet.* **2000**, *25*, 299−370.

(13) Harris, J. G. *J. Phys. Chem*. **1992**, *96*, 5077−5086.

(14) Mondello, M.; Grest, G. S. *J. Chem. Phys.* **1995**, *103*, 7156−7165.

(15) (a) Mundy, C. J.; Balasubramanian, S.; Bagchi, K.; Siepmann, J. I.; Klein, M. L. *Faraday Discuss.* **1996**, *104*, 17−36. (b) Zhuravlev, N. D.; Siepmann, J. I. *Fluid Phase Equil.* **1997**, *134*, 55−61. (c) Zhuravlev, N. D.; Martin, M. G.; Siepmann, J. I. *Fluid Phase Equilib.* **2002**, *202*, 307−324.

(16) Wick, C. D.; Siepmann, J. I.; Schure, M. R. *Anal. Chem.* **2002**, *74*, 3518−3524.

(17) Martin, M. G.; Siepmann, J. I. *J. Phys. Chem. B* **1999**, *103*, 4508−4517.

(18) Poncela, A.; Rubio, A. M.; Freire, J. *J. Mol. Phys.* **1997**, *91*, 189−202.

(19) Smith, W.; Forester, T. R. DL_POLY (version 2.14) http://www.cse.clrc.ac.uk/msi/software/DL_POLY, Daresbury Laboratory, 2003.

(20) Hoover, W. G. *Phys. Rev. A* **1985**, *31*, 1695−1697.

(21) Kuznetsova, T.; Kvamme, B. *Phys. Chem. Chem. Phys.* **2002**, *4*, 937−941.

(22) Phillips, L. F. *J. Phys. Chem. B* **2004**, *108*, 1986−1991.

(23) Townsend, R. M.; Gryko, J.; Rice, S. A. *J. Chem. Phys.* **1985**, *82*, 4391−4392.

(24) Allen, M. P.; Tildesley, D. J. *Computer Simulation of Liquids*; Oxford University Press: Oxford, 1993.

(25) Baker, R. P.; Costen, M. L.; Hancock, G.; Ritchie, G. A. D.; Summerfield, D. *Phys. Chem. Chem. Phys.* **2000**, *2*, 661−664.

(26) (a) Walch, S. P.; Dunning, T. H., Jr. *J. Chem. Phys.* **1980**, *72*, 3221−3227. (b) Luntz, A. C.; Andresen, P. *J. Chem. Phys.* **1980**, *72*, 5851−5856. (c) Gonzáles, M.; Hernando, J.; Millán, J.; Sayós, R. *J. Chem. Phys.* **1999**, *110*, 7326−7338. (d) Espinosa-García, J.; García-Bernáldez, J. C. *Phys. Chem. Chem. Phys.* **2000**, *2*, 2345−2351. (e) Yan, T.; Hase, W. L.; Doubleday, C. *J. Chem. Phys.* **2004**, *120*, 9253−9265.

(27) (a) Li, G.; Bosio, S. B. M.; Hase, W. L. *J. Mol. Struct.* **2000**, *556*, 43−57. (b) Troya, D.; Schatz, G. C. *J. Chem. Phys.* **2004**, *120*, 7696−7707.